Measurement of α and neutron decay widths of excited states of ^{14}C

P. J. Haigh,[1,*] N. I. Ashwood,[1] T. Bloxham,[1] N. Curtis,[1] M. Freer,[1] P. McEwan,[1] D. Price,[1] V. Ziman,[1] H. G. Bohlen,[2] Tz. Kokalova,[2] Ch. Schulz,[2] R. Torabi,[2] W. von Oertzen,[2] C. Wheldon,[2] W. Catford,[3] C. Harlin,[3] R. Kalpakchieva,[4] and T. N. Massey[5]

[1]*School of Physics and Astronomy, University of Birmingham, Edgbaston, Birmingham, B15 2TT, United Kingdom*

[2]*Hahn-Meitner-Institut, Glienicker Strasse 100, D-14109 Berlin, Germany*

[3]*The School of Electronics and Physical Sciences, University of Surrey, Guildford, Surrey, GU2 7XH, United Kingdom*

[4]*Flerov Laboratory, JINR, RU-141980 Dubna, Russia*

[5]*Department of Physics and Astronomy, Ohio University, Athens, Ohio 45701-2979, USA*

(Received 13 February 2008; published 25 July 2008)

The ^{12}C(^{16}O,^{14}O)^{14}C reaction was studied at a beam energy of 234 MeV. The ^{14}O ejectile was detected by a Q3D spectrometer at forward angles. The energies and angles of the excited ^{14}C recoil break-up fragments were measured in coincidence with the ^{14}O ejectile using a double sided silicon strip detector array at backward angles. A complete kinematic reconstruction of the reaction was performed to reconstruct the $^{14}C^* \rightarrow {}^{10}\mathrm{Be} + \alpha$ and $^{14}C^* \rightarrow {}^{13}\mathrm{C} + n$ decay channels and the branching ratios and widths of these decays were calculated. Theoretical decay branches were calculated using barrier penetrability factors and were compared to the measured ratios to provide information on the spins, parities, and configurations of the states. Neutron emission was found to be favored for the 11.73, 12.96, 14.87, 16.72, and 18.6 MeV states. The 14.87, 18.6, and 21.4 MeV states were found to have a considerable width for α-decay and are candidates for the three bodied molecular cluster structure of ^{14}C.

DOI: 10.1103/PhysRevC.78.014319 PACS number(s): 21.10.Tg, 21.60.Gx, 23.60.+e, 27.20.+n

I. INTRODUCTION

It is well known that ^{8}Be has a well developed α-α cluster structure [1,2]. The ^{8}Be nucleus is unstable as the α-α interaction is weak and has a repulsive core due to the Pauli principle. However, the addition of a neutron produces enough binding energy to make the ^{9}Be nucleus stable. The binding energy which stabilizes the system is provided by the neutron which resides in delocalized orbits around the α-cores. In the case of ^{10}Be, linear combinations of the two valence neutron orbitals produce π- and σ-bonds which bind the dimer core [3]. There is now strong evidence for these molecular-like α-cluster structures in ^{9,10}Be [4–10]. Antisymmetrized molecular dynamics (AMD) calculations provide further support for these molecular structures in $^{9-12}$Be; where they reproduce these molecular characteristics despite the fact that no explicit cluster content is assumed [3,11–16].

These concepts can be extended to the neutron-rich carbon isotopes, in which the core has a three α-particle cluster configuration. Again, the valence neutrons would reside in delocalised molecular orbits around the cores and would increase the binding energy and stability of the system. These ideas have been explored extensively by Milin and von Oertzen *et al.*, in which the complete spectroscopy of ^{13}C [17] and ^{14}C [18] states were examined. In this method, the single-particle shell-model states are eliminated and the remaining states are assigned to rotational bands associated with prolate, linear-chain structures and oblate, triangular configurations. In ^{14}C, three different molecular cluster configurations can be expected: triangular configurations with the neutrons in σ-bonds between two of the α-particles, linear reflection-symmetric chains in which the valence neutrons are equally distributed among the three α-cores (α-n-α-n-α) and linear intrinsically reflection-asymmetric configurations in which the two neutrons reside between two of the α-cores (α-2n-α-α). This final configuration gives rise to parity inversion doublets.

These proposed molecular configurations should exhibit strong α-decay. Here we present measurements of the neutron and α-decay branching ratios associated with highly excited states in ^{14}C. The experimentally determined branching ratios are compared with theoretical decay branches to provide information on the spins, parities, and configurations of these states. Additional information on the widths and population of the states, which depend on dynamical matching conditions, are used to help indicate their properties.

II. EXPERIMENTAL PROCEDURE

The two-neutron transfer reaction ^{12}C(^{16}O,^{14}O)^{14}C was studied at a beam energy of 234 MeV, in two separate measurements, at the Ionen-Strahl-Labor (ISL) facility, at the Hahn-Meitner-Institut (HMI), Berlin. This reaction has a ground state Q-value of $Q_0 = -15.763$ MeV. In the first set of measurements the beam was incident on a 200 μg cm^{-2} ^{12}C target and in the second the target used was a 20 μg cm^{-2} ^{12}C foil.

The measurements were performed with a Q3D magnetic spectrometer [19–21] and an array of charged particle detectors. The ^{14}O ejectile was identified in the Q3D focal plane detector using proportional wires for energy loss and a plastic scintillator to measure time of flight and total energy. The position of the ^{14}O along the focal plane was measured using the delay-line read-out technique. The ^{14}O nucleus has no

*pjh@np.ph.bham.ac.uk

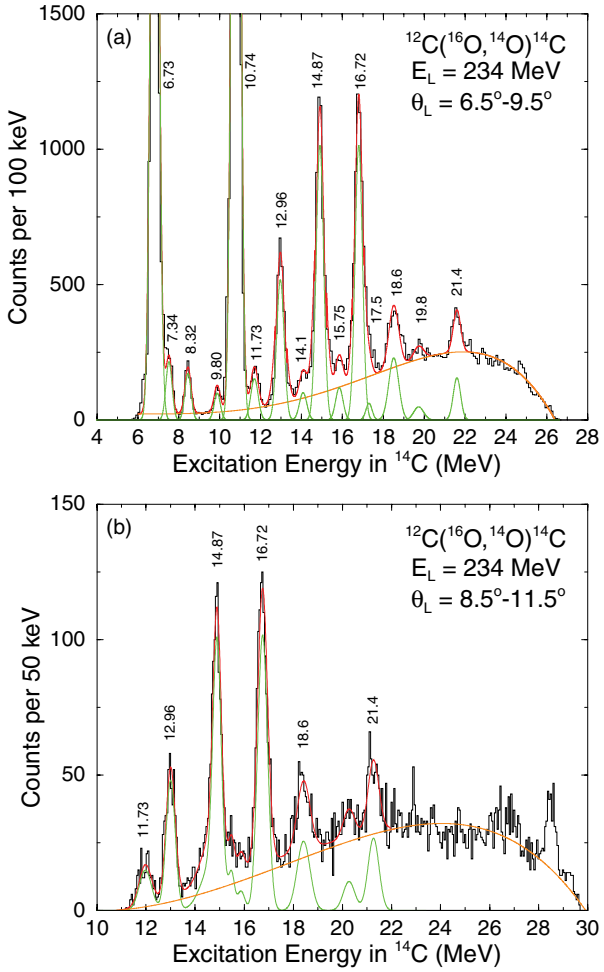

FIG. 1. (Color online) The ^{14}C excitation energy spectra fitted with Gaussian peaks, whose centroids are indicated, and a smooth background. The peaks ranging from 6.73 to 21.4 MeV represent the ^{14}C states populated in the two-neutron transfer reaction ^{12}C(^{16}O,^{14}O)^{14}C. The angular range of the Q3D acceptance aperture is indicated. In (b) the magnetic-field settings of the Q3D have been chosen to emphasize the higher-excitation-energy region. The feature at 28.4 MeV is not an excited state, but rather an edge effect at the low-energy side of the detector.

bound excited states and thus its position along the focal plane yields the excitation energy of the ^{14}C nucleus, as shown in Fig. 1. In the first set of measurements, the magnetic rigidity of the Q3D spectrometer was set to observe ^{14}C states with excitation energies 6.73 to 21.4 MeV (a). In the second set of measurements, the spectrometer was set for the excitation energy range 11.73 to 21.4 MeV (b).

The distance traveled by a particle within the Q3D spectrograph primarily depends on its emission angle. Hence the time of flight depends on the length of the trajectory and can thus be used to deduce the scattering angle within the horizontal acceptance aperture of the Q3D. Due to the excellent time resolution an angular resolution of 0.3° was achieved. The scattering angle of the ^{14}O and the excitation energy of the ^{14}C can be used to determine the laboratory energy of the ^{14}O and thus a complete reconstruction of the binary reaction can be performed.

The decay products of the excited ^{14}C recoil were detected, in coincidence with the ^{14}O ejectile, using an array of solid state charged particle detectors. This array initially comprised two 50 mm × 50 mm double sided silicon strip detectors (DSSSD) approximately 500 μm thick and for the second set of measurements was composed of four such detectors. Each detector face was subdivided into 16 independent 3 mm wide strips, with the direction of the strips on the front face being perpendicular to those on the back. Hence each detector was essentially formed from 256, 9 mm^2, pixels. The detectors had an angular resolution of $\Delta\theta_{\rm lab} \leqslant 1.3^\circ$ and a typical energy resolution of 150 keV. For the first set of measurements three different angular arrangements of the spectrometer and the DSSSDs were used and for the second measurement, only one setting was used. The details of the various experimental setups are shown in Table I.

III. ANALYSIS AND RESULTS

Below 20.6 MeV the excited ^{14}C nucleus only has two available decay channels: ^{10}Be + α($E_{\rm thresh}$ = 12.01 MeV) and ^{13}C + n($E_{\rm thresh}$ = 8.18 MeV). The majority of ^{14}O events detected in the spectrometer were in coincidence with only one ^{14}C decay product in the DSSSD array. Thus, particles detected in the DSSSD array were assumed to be either ^{13}C or ^{10}Be nuclei. For both decay channels momentum conservation was used to reconstruct the energy and the angle of the undetected breakup particle and the three-body Q-value, Q_3, was calculated as

$$Q_3 = E_{^{14}\rm O} + E_{\rm D_1} + E_{\rm D_2} - E_{\rm beam}, \qquad (1)$$

where D_1 and D_2 represent the two decay products of the excited ^{14}C recoil. The excitation energy of the breakup

TABLE I. Details of the detector arrangements for the various measurements. The angles (θ_x, θ_y) and distances are measured from the center of the reaction target to the center of the associated detector.

Setup	Q3D angle (degrees)	θ_x, θ_y (degrees), distance (mm)											
		DSSSD1			DSSSD2			DSSSD3			DSSSD4		
1	10.5–13.5	73.0	0.0	169.5	50.5	0.0	169.5						
2	10.5–13.5	55.5	0.0	169.5	33.0	0.0	169.5						
3	6.5–9.5	59.5	0.0	169.5	37.0	0.0	169.5						
4	8.5–11.5	47.5	13.1	142.7	47.5	−10.1	141.2	25.0	11.4	167.3	25.0	−8.4	165.8

fragments was calculated by comparing Q_3 with the three-body Q-value in which the decay products are produced in their ground states, Q_{3_0}:

$$E_x(D_{1,2}) = |Q_{3_0} - Q_3|. \quad (2)$$

In each decay channel only one of the daughter nuclei can be in an excited state, as the first excited state of an α particle is 20.2 MeV. Thus, the excitation energy of the breakup fragments corresponds to the excitation energy of either the ^{13}C or the ^{10}Be. So, for example, the detection of a ^{10}Be nucleus with $E_x(^{10}\text{Be}) = 3.368$ MeV corresponds to the $^{14}\text{C}^*\alpha$-decaying to the first excited state of ^{10}Be.

The various decay channels were analyzed using Monte Carlo simulations of the reaction and detection processes. The simulations reproduce the experimental acceptances and smear the energies and angles in accordance with the experimental resolutions. The outputs of the simulations were subsequently processed as if they were real events using the same analysis procedures as those used for the experimental data. These simulations permitted the theoretical peak line-shapes in the decay products excitation energy spectra to be reconstructed. These line-shapes were normalized to fit the experimental data and the integrated area of the line-shapes were compared with the number of counts in the associated state in the Q3D, ^{14}C, excitation energy spectrum, in order to deduce branching ratios.

Figure 2 shows the ^{13}C excitation energy spectra, produced for various ^{14}C states by gating on the appropriate peak in the ^{14}C excitation energy spectrum [Fig. 1(a)]. The spectra are obtained from the measurements involving setup 3 (Table I), after the coincident detection of the ^{13}C decay fragment and the ^{14}O ejectile and assuming a missing neutron. The histograms correspond to the experimental data. The peaks centered at $E_x(^{13}\text{C}) = 0$ MeV correspond to the $^{14}\text{C}^*$ decaying via neutron emission to the ground state of ^{13}C. The peaks centered at $E_x(^{13}\text{C}) \sim 3.8$ MeV correspond to events in which the $^{14}\text{C}^*$ decays to one of the first three excited states in ^{13}C. These three states are the $J^\pi = 1/2^+(3.089\,\text{MeV}), 3/2^-(3.6845\,\text{MeV})$ and $5/2^+(3.854\,\text{MeV})$ and are unresolved in the spectra. The ^{13}C excitation energy spectra (Fig. 2) and the ^{14}C excitation energy spectra (Fig. 1) were used to calculate the branching ratios for the neutron decay of the $^{14}\text{C}^*$ nuclei to various states in ^{13}C.

The relative branching ratio, BR_{rel}, of a particular ^{14}C state, is the ratio between the decay rates, N_A and N_B, of two different individual decay channels of that state and is

$$\text{BR}_{\text{rel}} = \frac{N_A/\varepsilon_A}{N_B/\varepsilon_B}, \quad (3)$$

where ε is the detection efficiency and is given by the Monte Carlo simulations. The values of N_A and N_B, are given by the number of counts in the associated peaks, in the decay fragments excitation energy spectrum (DSSSD counts). As noted, the number of counts in a peak was calculated by integrating the normalized function which corresponds to the peak line-shape. The absolute branching ratio, BR_{abs}, is the ratio between the decay rate, N_A, of an individual decay channel of a particular ^{14}C state and the total decay rate, N_T, of that state and is

$$\text{BR}_{\text{abs}} = \frac{N_A/\varepsilon_A}{N_T} = \frac{\text{No. of Counts in DSSSD}/\varepsilon_{\text{A}}}{\text{No. of Counts in Q3D Detector}}. \quad (4)$$

The value of N_T, for the ^{14}C state being studied, is given by the number of counts in the associated peak, in the ^{14}C excitation energy spectrum (Q3D counts).

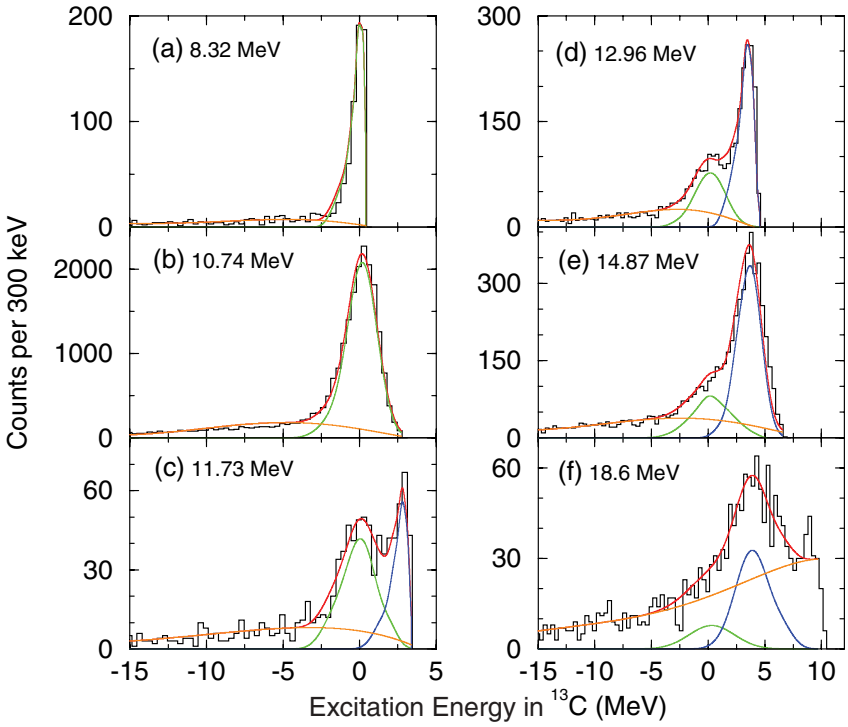

FIG. 2. (Color online) ^{13}C states populated in the decay of excited states in ^{14}C. The spectra are produced by gating on the appropriate peak in the ^{14}C excitation energy spectrum [Fig. 1(a)] following the coincident detection of the ^{14}O ejectile and the ^{13}C decay fragment and assuming a missing neutron. The spectra are obtained from the setup 3 (Table I) measurement and are fitted with the simulated peak line-shapes and a smooth polynomial background. In each spectrum the excitation energy of the decaying ^{14}C state is indicated.

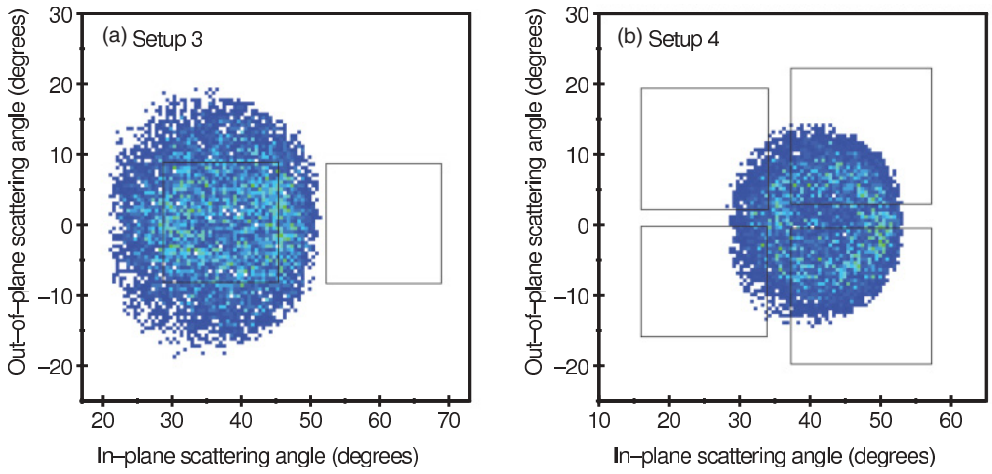

FIG. 3. (Color online) The simulated angular distribution of the ^{13}C decay fragments for the measurements involving setups 3 and 4. The outlines of the DSSSDs are shown.

A. Detection efficiencies

To calculate the branching ratios, the detection efficiencies must be calculated using the simulations. As an example, the ^{12}C(^{16}O,^{14}O)^{14}C*[^{13}C + n] reaction was simulated for the 12.96 MeV ^{14}C* state, for setup 3 (two DSSSDs). The in-plane and out-of-plane angles of the ^{13}C decay fragments with respect to the beam direction are shown in Fig. 3(a). The outlines of the DSSSDs are shown. The 'breakup circle' formed by the detection of the ^{13}C nuclei is clearly evident. Events which fall outside of the active area of the detectors are rejected and the detection efficiency, ε, is given by

$$\varepsilon = \frac{\text{No. of Events Detected in the DSSSD Array}}{\text{No. of Events Detected in the Q3D Spectrometer}}. \quad (5)$$

As the spins of many of the states are unknown the simulations are performed assuming an isotropic decay. In reality the decay is anisotropic, resulting in a slightly different angular distribution of the decay fragments. This will affect the distribution of the yield across the breakup circle. From Fig. 3(a) it is evident that only a fraction of the ^{13}C decay fragments are detected. The fraction of detected particles depends on the angular distribution of these particles and thus, for large breakup cones an error is introduced into the efficiency calculations and subsequently into the branching ratios. This is not a problem for the lower energy ^{14}C* states (E_x(^{14}C) < 10.74 MeV) as the detection efficiencies are very close to 100%. Similarly, the detection efficiencies are also close to 100% for ^{14}C* states, with E_x(^{14}C) $\leqslant$12.96 MeV, which decay to excited states in ^{13}C. However, as the excitation energy of the ^{14}C increases, the detection efficiencies of the decay fragments decrease and the effect of this problem increases. This is accentuated for the ^{10}Be + α decay channel as the ^{10}Be decay fragments are emitted with a greater angular range than the ^{13}C decay fragments.

The second experiment described (setup 4), used a silicon array constructed from four detectors. Figure 3(b) shows the simulated angular distribution of the ^{13}C nuclei, emitted in their ground states from the ^{14}C* nuclei (E_x(^{14}C) = 12.96 MeV). With the exception of the dead areas between the detectors, the entire angular distribution is observed. The improvement in the observation of a greater fraction of the angular distribution is mainly achieved by simply increasing the number of detectors. However, it is also improved by reducing the size of the breakup circle with respect to the detectors. In a comparison between Figs. 3(a) and 3(b), it is evident that the breakup circle is indeed smaller in the measurements involving setup 4. This is achieved in two ways. Firstly, the detectors were moved closer to the target at the expense of the angular resolution. Secondly, the angle of the Q3D spectrometer was increased. As the Q3D angle increases, the energy of the ^{14}C increases, thus reducing the size of the breakup cone. The one disadvantage is that the number of detected ^{14}O particles exponentially decreases as the scattering angle increases and thus the statistical uncertainties increase. For the four DSSSD setup, the entire breakup circle of the ^{13}C decay fragments falls within the limits of the array, for all the ^{14}C states studied. Thus, the errors introduced into the detection efficiency calculations, by the assumption of an isotropic decay, are significantly reduced for setup 4 and the branching ratios can be calculated without the need to know the spin of the decaying ^{14}C state.

B. Experimental uncertainties and background contributions

From Eqs. (3), (4), and (5) it is clear that the branching ratios depend on the number of counts in the Q3D spectrometer, the number of counts in the DSSSDs and the detection efficiencies. Each of these values have inherent statistical errors which are associated with any random process. However, the statistical errors associated with the detection efficiencies are negligible as the simulations were run for a large number of events. In addition, there are systematic errors associated with the uncertainty in the smooth background fit to the data, and the parameters used in the simulations.

In several cases, the dominant source of error in the number of counts in the DSSSD array arises from the fitting of the simulated line-shapes, and background functions, to the experimental data. Figure 2(c) shows the ^{13}C states populated in the decay of the 11.73 MeV ^{14}C state. The two peaks are

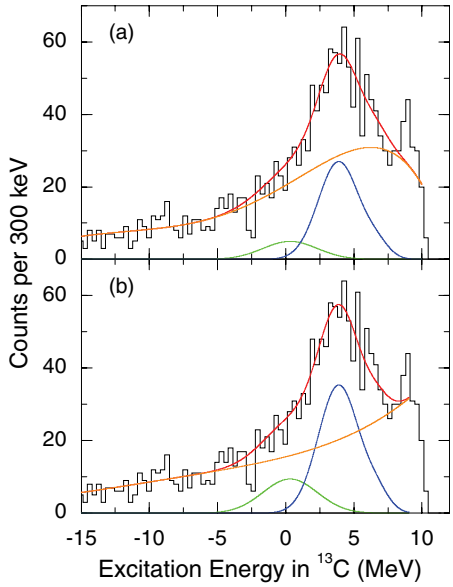

FIG. 4. (Color online) Two possible fits for the peak line-shapes and background to the ^{13}C states populated in the decay of the 18.6 MeV ^{14}C state.

well resolved and the background contribution is smooth and small. As a consequence, errors in the fitting process are small. Figure 4, on the other hand, shows two possible ways of fitting the line shapes and backgrounds to the ^{13}C states populated in the decay of the 18.6 MeV ^{14}C state. In this case the fitting process is far more subjective resulting in larger errors. These errors are especially a problem in the ^{10}Be excitation energy spectra, where the peaks lie on large and uneven backgrounds.

To reduce these 'fitting' errors, analysis was performed to understand the shapes of the backgrounds, in the excitation energy spectra of the decay fragments. One contribution to the background arises from the lack of particle identification. Thus, ^{10}Be events were processed as ^{13}C events in the ^{13}C+n analysis and vice versa. Monte Carlo simulations were performed to analyze the background contributions that arise from this ambiguity. It was found that ^{10}Be events analyzed as ^{13}C events, would produce an even, low-lying background in the ^{13}C excitation energy spectra. Thus, peaks in the ^{13}C excitation energy spectra lie on this even background and are largely unaffected. Conversely, ^{13}C events analyzed as ^{10}Be events, produce a background in which the counts are bunched up in the higher ^{10}Be excitation energy region.

The second contribution to the background arises from the coincident detection of background events in the Q3D and background events in the DSSSD array. To determine the approximate shape of such background contributions, regions of the ^{14}C excitation energy spectra, in which there are only background events, are analyzed as if they were real excited states. For example, in the ^{14}C excitation energy spectra (Fig. 1), the region between the 19.8 and 21.4 MeV peaks contains Q3D background counts only. These counts were analyzed as a 20.6 MeV ^{14}C state and the decay products excitation energy spectra were obtained. The histograms produced gave an approximate shape of the background contribution for the 18.6 and 21.4 MeV states.

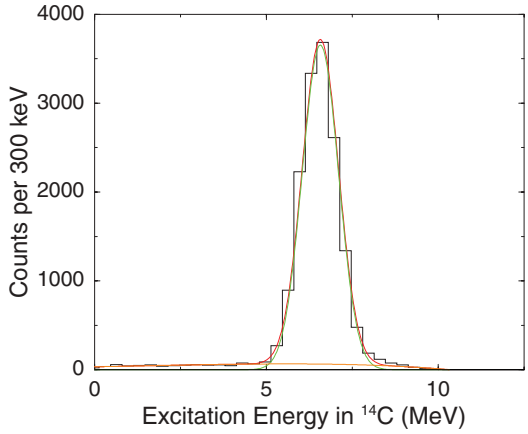

FIG. 5. (Color online) The 6.73 MeV ^{14}C state populated in the ^{12}C(^{16}O,^{14}O)^{14}C reaction. The spectrum is obtained after the coincident detection of the ^{14}C*, in the DSSSD array, with the ^{14}O ejectile, in the Q3D. The data is fitted with a simulated peak line-shape and a smooth background.

C. The binary reaction

The 6.73 MeV ^{14}C state is strongly populated in the two neutron transfer reaction as shown in Fig. 1. The state is bound and thus the ^{14}C nucleus is detected directly in the DSSSD array after it undergoes γ-decay. This provides a means of testing the procedure by which the detection efficiencies are calculated. Simulations show that the efficiency of detecting this state in the DSSSD array is 95–100%. Figure 5 shows the ^{14}C excitation energy spectrum, obtained after the coincident detection of the excited ^{14}C nuclei and the ^{14}O ejectile. The ratio of the number of hits in the Q3D focal plane to the number of 6.73 MeV ^{14}C hits in the DSSSD array is 0.96 $\pm$ 0.10. As expected, the experimental detection efficiency and the simulated detection efficiency are equal within errors.

D. The ^{13}C + n decay channel

Figure 6 shows the ^{14}C states which have sufficient excitation energy to decay via the ^{13}C + n channel. The ^{13}C states populated in the decay of excited states in ^{14}C are shown in Figs. 2 and 7. The two sets of spectra are obtained with measurements from setup 3 and 4, respectively, after the coincident detection of the ^{13}C decay fragment and the ^{14}O ejectile and assuming a missing neutron. The branching ratios for the neutron decays of excited ^{14}C states are shown in Table II and the decay widths are shown in Table III.

The 8.32 MeV and 10.74 MeV ^{14}C states only have sufficient excitation energy to neutron decay to the ground state of ^{13}C. Thus, these two states provide a good method for testing the validity of the procedure used to calculate the branching ratios. The ^{13}C excitation energy spectra for these two states are shown in Figs. 2(a) and 2(b), respectively. The peaks centered at $E_x(^{13}\mathrm{C}) = 0$ MeV correspond to the ^{13}C nuclei being emitted in their ground states. Using Eq. (4), the absolute branching ratios, for the decay of the 8.32 MeV and

TABLE II. The branching ratios for the decay of excited ^{14}C states via the $^{13}C + n$ and $^{10}Be + \alpha$ channels. For the neutron channel the branching ratios are shown for the decay to the $^{13}C[1/2^-]$ ground state (g.s.) and the $1/2^-$(3.089 MeV), $3/2^-$(3.6845 MeV) and $5/2^+$(3.854 MeV) first three excited states ($ES_{1,2,3}$). For the α-channel the branching ratios are shown for the decay to the $^{10}Be[0^+]$ ground state (g.s.), the 2^+(3.3680 MeV) first excited state (ES_1) and the 2^+, 1^-, 0^+ and 2^- quartet at ~6 MeV ($ES_{2,3,,5}$).

^{14}C state (MeV)	$^{13}C + n$		$^{10}Be + \alpha$		
	g.s.	$ES_{1,2,3}$	g.s.	ES_1	$ES_{2,3,4,5}$
8.32	1.02 ± 0.09				
10.74	1.03 ± 0.03				
11.73	0.72 ± 0.04	0.28 ± 0.04			
12.96	0.34 ± 0.06	0.59 ± 0.08	<0.10		
14.87	0.21 ± 0.04	0.57 ± 0.08	0.16 ± 0.03		
18.6	<0.21	0.57 ± 0.16	<0.10	0.33 ± 0.10	<0.05
21.4	<0.05	<0.05	<0.10	0.66 ± 0.15	0.22 ± 0.07

10.74 MeV states to the ground state of ^{13}C, are calculated to be 1.02 ± 0.09 and 1.03 ± 0.03, respectively. Thus, these values are both equal to one, as expected.

For the 11.73 MeV, ^{14}C state, the peak centered at $E_x(^{13}C) = 3.089$ MeV corresponds to events in which the ^{14}C decays to the 3.089 MeV first excited state in ^{13}C. For the excited ^{14}C states, with $E_x(^{14}C) \geqslant 12.96$ MeV, the peaks centered at $E_x(^{13}C) \sim 3.8$ MeV correspond to events in which the $^{14}C^*$ decays to one of the first three excited states in ^{13}C. The 3.089, 3.6845, and 3.854 MeV states have a separation of 765 keV and are unresolved.

From Fig. 6, it is clear that the $^{14}C^*$ states with $E_x(^{14}C) \geqslant 16.72$ MeV have sufficient excitation energy to neutron decay to ^{13}C states which lie above the $^{12}C+n$ decay threshold. A ^{13}C nucleus emitted in one of these excited states will subsequently neutron decay to ^{12}C. In such an event the ^{12}C nucleus detected in the DSSSD is analyzed as a ^{13}C nucleus. Thus, these events will contribute to the backgrounds in the ^{13}C and ^{10}Be excitation energy spectra. As an example, a simulation was performed to study the reaction in which a 16.72 MeV ^{14}C state neutron decays to a 6.864 MeV ^{13}C state, which subsequently neutron decays to the ground state of ^{12}C. In order to model this process the outputs of the simulations, which represent the energies and angles of the ^{12}C, were analyzed as if they were ^{13}C nuclei and the ^{13}C excitation energy spectrum was produced [Fig. 8(a)]. The two vertical lines represent the positions of the ground state and the 3.854 MeV energy levels of the ^{13}C. The ^{13}C excitation energy spectrum obtained from the setup 4 data set, for the decay of the 16.72 MeV ^{14}C state is shown in Fig. 8(b). In a comparison between the two spectra it is evident that the histograms have a similar shape. Thus it is not possible to determine if the peak centered at $E_x(^{13}C) \sim 3.8$ MeV corresponds to the ^{14}C decaying to a bound excited state in ^{13}C or to the ^{12}C ground state. Thus the $^{13}C + n$ branching ratios cannot be determined for the 16.72 MeV state. However, by analyzing the number of counts in the broad peak in Fig. 8(b), it can be concluded that the 16.72 MeV state has a significant width for decay to excited states in ^{13}C. The decay to the ^{13}C ground state is not observed. Similar simulations show that the ^{12}C background is not a problem for the $^{14}C^*$ states with $E_x(^{14}C) \geqslant 18.6$ MeV.

The ^{13}C ground state is weakly populated in the decay of the 18.6 MeV ^{14}C state. It is evident from Fig. 7(c) that the ground-state peak lies on a large background and contains a limited number of counts. As a consequence the uncertainties associated with the fitting procedure are large for this particular decay channel. Thus, the branching ratio is quoted as an upper limit.

The decay of the 21.4 MeV ^{14}C state via the $^{13}C + n$ channel is not observed.

TABLE III. The neutron and α-decay widths of excited states in ^{14}C. The total decay widths are taken from Ref. [18].

^{14}C State (MeV)	$^{13}C + n$ decay width (keV)		$^{10}Be + \alpha$ decay width (keV)			Total decay width (keV)
	g.s.	$ES_{1,2,3}$	g.s.	ES_1	$ES_{2,3,4,5}$	
8.32	3.40					3.4
10.74	10.00					10
11.73	21.60 ± 1.20	8.40 ± 1.20				30
12.96	8.50 ± 1.50	14.75 ± 2.00	<2.50			25
14.87	7.35 ± 1.40	19.95 ± 2.80	5.60 ± 1.05			35
18.6	<21.00	57.00 ± 16.00	<10.00	33.00 ± 10.00	<5.00	100
21.4	<27.50	<27.50	<55.00	363.00 ± 82.50	121.00 ± 38.50	550

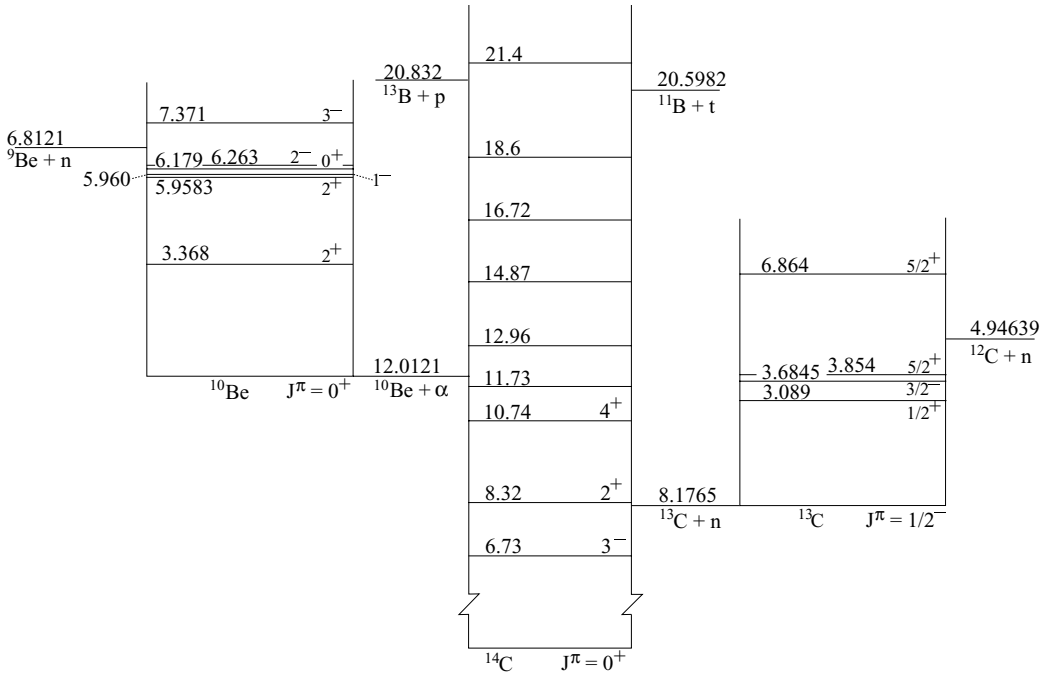

FIG. 6. An energy level diagram illustrating the possible decay channels available to various ^{14}C states. The energy thresholds for the various decay channels are indicated.

E. The ^{10}Be + α decay channel

Figure 6 shows the ^{14}C* states which have sufficient excitation energy to decay via the ^{10}Be + α channel. The ^{10}Be states populated in the decay of excited states in ^{14}C are shown in Fig. 9. The branching ratios and α-decay widths of various excited ^{14}C states are shown in Tables II and III, respectively.

1. Multiplicity 1 events

The spectra in Fig. 9(a)–9(c) are obtained from the setup 4 data set (Table I), after the coincident detection of the ^{14}O in the Q3D spectrometer, with the ^{10}Be in the DSSSD array and assuming a missing α-particle.

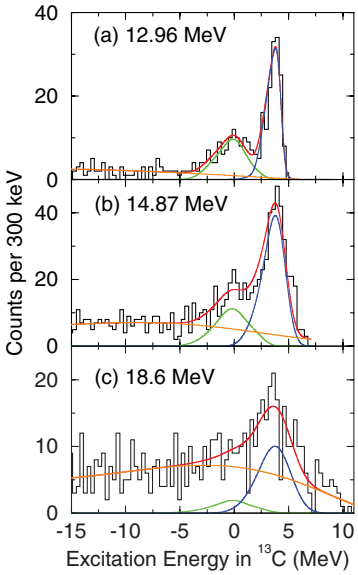

FIG. 7. (Color online) ^{13}C excited states populated in the decay of excited states in ^{14}C. The excitation energy of the decaying ^{14}C state is indicated. The spectra are obtained from the measurement involving setup 4 (Table I) and are fitted with the simulated peak line-shapes and a smooth polynomial background.

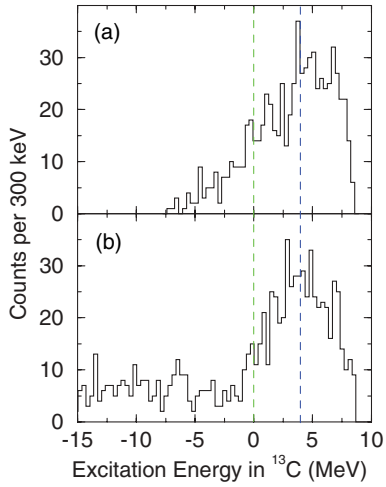

FIG. 8. (Color online) (a) shows the simulated ^{13}C excitation energy spectrum obtained following the detection of ^{12}C nuclei which are analyzed as if they were ^{13}C nuclei. The energies and angles of the ^{12}C were obtained from Monte Carlo simulations of the ^{14}C*(16.72 MeV) $\rightarrow$ ^{13}C*(6.864 MeV) + n, ^{13}C*(6.864 MeV) $\rightarrow$ ^{12}C + n reaction. (b) shows the ^{13}C excitation energy spectrum obtained from the setup 4 data set, following the coincident detection of the ^{14}O with one of the 16.72 MeV ^{14}C decay fragments and assuming a missing neutron.

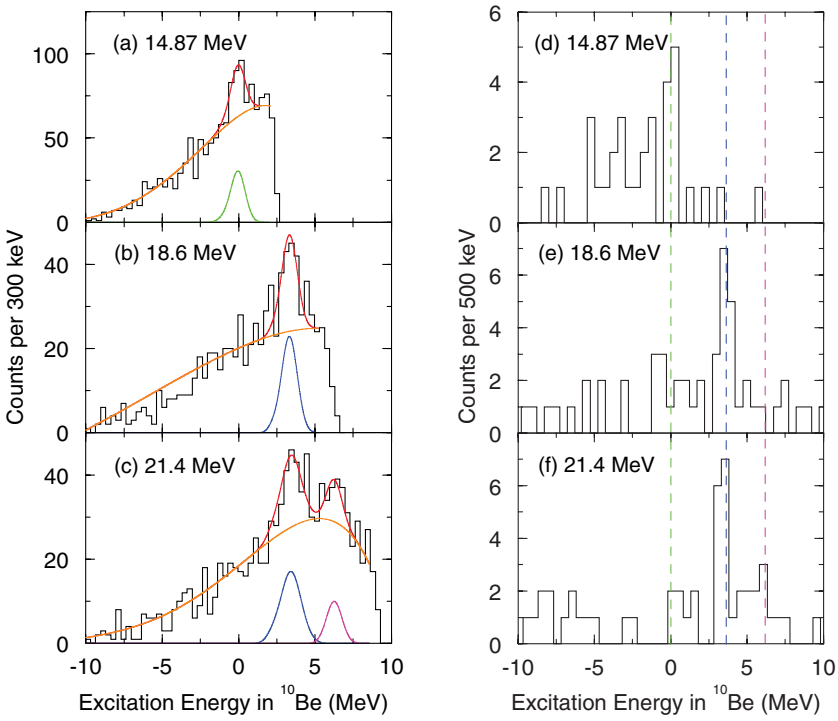

FIG. 9. (Color online) ^{10}Be excited states populated in the decay of excited states in ^{14}C. The multiplicity 1 spectra [(a)–(c)] are obtained after the coincident detection of the ^{14}O ejectile and the ^{10}Be decay fragment and assuming a missing α-particle. The data are fitted with the simulated peak line shapes and a smooth polynomial background. The multiplicity 2 spectra [(d)–(f)] are obtained following the coincident detection of the three final state particles. The vertical lines represent the positions of the ground state, the 3.3680 MeV and the 5.960 MeV energy levels of ^{10}Be. The excitation energy of the decaying ^{14}C state is indicated.

It has already been noted that ^{13}C events form backgrounds in the ^{10}Be excitation energy spectra which are compressed into the higher excitation-energy regions. For the 12.96 MeV state, this region coincides with the ^{10}Be ground state energy. Consequently, the ^{13}C background forms a peak at $E_x(^{10}\mathrm{Be}) \sim 0$ MeV and thus it is not possible to determine if the 12.96 MeV ^{14}C state decays via the $^{10}\mathrm{Be} + \alpha$ branch. However, from the $^{13}\mathrm{C} + n$ analysis (Table II) it is evident that this branch must be small if it exists at all.

For the 14.87 MeV state of ^{14}C the peak centered at $E_x(^{10}\mathrm{Be}) = 0$ MeV [Fig. 9(a)] corresponds to the α-decay to the ground state of ^{10}Be.

The 16.72 MeV ^{14}C state has sufficient excitation energy to α-decay to both the ground state and first excited state in ^{10}Be. However, a significant width for decay via the $^{10}\mathrm{Be} + \alpha$ branch is not observed. Thus it is concluded that the dominant decay mode for this state is neutron decay.

The 18.6 MeV ^{14}C state has sufficient excitation energy to α-decay to ^{10}Be states with $E_x(^{10}\mathrm{Be}) < 6.589$ MeV. In Fig. 9(b) the peak centered at $E_x(^{10}\mathrm{Be}) = 3.368$ MeV corresponds to the ^{10}Be nuclei being emitted in the first excited state. The α-decay to the ^{10}Be ground state and to the group of states at $E_x(^{10}\mathrm{Be}) \sim 6$ MeV is not observed.

The 21.4 MeV state of ^{14}C has a substantial width for the α-decay to both the first excited state in ^{10}Be and the group of states at $E_x(^{10}\mathrm{Be}) \sim 6$ MeV. The peak centered at $E_x(^{10}\mathrm{Be}) \sim 6$ MeV corresponds to the $^{14}\mathrm{C}^*$ decaying to either the 5.9583, 5.960, 6.179, or 6.263 MeV, ^{10}Be states, which are unresolved. The decay to the ^{10}Be ground state is not observed. The 21.4 MeV ^{14}C state has sufficient excitation energy to α-decay to the 7.371, 7.542, and 9.27 MeV states. These states lie above the $^{9}\mathrm{Be}+n$ decay threshold ($E_{\mathrm{thresh}} = 6.8121$ MeV) and will subsequently neutron decay to ^{9}Be. The two neutrons produced in such a decay are not observed and, therefore, the reaction Q-value cannot be determined for such decays.

2. *Multiplicity 2 events*

There were a number of events in which the ^{14}O ejectile was detected in coincidence with both the ^{10}Be and α decay products. In such events the energies of the three final-state particles are measured directly and the Q-value and excitation energies of the decay fragments are calculated using Eqs. (1) and (2). In order to accurately reproduce the excitation energies of the decay fragments the energy lost by the particles in traversing the target must be calculated and added to the energy of the detected particle. However, this is impossible as the identification of the decay fragments is ambiguous. Thus, such calculations can only be performed if the target is thin enough that the energy loss is smaller than the energy resolution and can thus be ignored. This was the case for the measurements involving setup 4, in which the target was 20 μg cm^{-2}. The ^{10}Be excitation energy spectra, produced after the coincident detection of all of the three final-state particles are shown in Fig. 9(d)–9(f). In this instance the detection efficiency is small and thus the number of observed counts is reduced. The 12.96 MeV state was not observed to decay via the $^{10}\mathrm{Be} + \alpha$ branch. The peak in Fig. 9(d) corresponds to the 14.87 MeV ^{14}C state, α-decaying to the ground state of ^{10}Be. The two peaks in the 18.6 and 21.4 MeV spectra, centered at $E_x(^{10}\mathrm{Be}) \sim 3$ MeV, correspond to the decay of the ^{14}C to the first excited state in ^{10}Be. The decay of the 21.4 MeV state, to the group of ^{10}Be states with $E_x(^{10}\mathrm{Be}) \sim 6$ MeV, is not strongly observed. However, the population of this group of states is relatively weak and it is highly probable that it is

TABLE IV. The theoretical decay branch ratios for the neutron decay of various $^{14}C^*$ states to the ^{13}C ground state ($1/2^-$) as a fraction of the neutron decay to any of the first three excited states ($1/2^+$, $3/2^-$, $5/2^+$). The ratios are shown for $J_i = 0$ to 8 for both the even and odd parity states. The numbers in the brackets represent the strength of the $1/2^+$, $3/2^-$ and $5/2^+$ decay widths as a fraction of their total width. Also shown are the associated experimental relative branching ratios. A comparison between the experimental and theoretical ratios provides information on the spin, parity and structure of the decaying ^{14}C state.

J_i^π	E_x (MeV)				
	11.73	12.96	14.87	16.72	18.6
0^-	5.12 (1, 0, 0)	1.55 (0.75, 0.23, 0.02)	0.78 (0.51, 0.34, 0.15)	0.59 (0.44, 0.34, 0.22)	0.51 (0.40, 0.34, 0.26)
1^-	8.66 (1, 0, 0)	1.23 (0.34, 0.44, 0.23)	0.72 (0.26, 0.44, 0.30)	0.59 (0.24, 0.42, 0.34)	0.54 (0.23, 0.42, 0.36)
2^-	3.51 (1, 0, 0)	0.50 (0.37, 0.42, 0.21)	0.29 (0.33, 0.40, 0.27)	0.23 (0.31, 0.40, 0.29)	0.20 (0.30, 0.40, 0.30)
3^-	404.42 (1, 0, 0)	1.82 (0.14, 0.27, 0.59)	0.79 (0.19, 0.31, 0.50)	0.59 (0.20, 0.33, 0.48)	0.51 (0.19, 0.34, 0.47)
4^-	64.22 (1, 0, 0)	0.99 (0.32, 0.62, 0.06)	0.39 (0.31, 0.49, 0.20)	0.30 (0.31, 0.45, 0.24)	0.25 (0.31, 0.43, 0.27)
5^-		14.25 (0.03, 0.10, 0.87)	1.56 (0.06, 0.21, 0.73)	0.88 (0.11, 0.28, 0.61)	0.66 (0.15, 0.31, 0.55)
6^-		3.79 (0.25, 0.74, 0.01)	0.47 (0.21, 0.72, 0.07)	0.30 (0.24, 0.62, 0.14)	0.26 (0.27, 0.54, 0.19)
7^-		302.46 (0.02, 0.05, 0.93)	5.88 (0.02, 0.09, 0.90)	1.84 (0.03, 0.14, 0.84)	1.07 (0.04, 0.19, 0.76)
8^-		21.92 (0.28, 0.72, 0.00)	0.71 (0.14, 0.83, 0.03)	0.27 (0.15, 0.79, 0.06)	0.19 (0.17, 0.74, 0.09)
0^+	2.49(1, 0, 0)	0.87 (0.56, 0.33, 0.11)	0.54 (0.42, 0.34, 0.24)	0.46 (0.39, 0.34, 0.27)	0.43 (0.37, 0.34, 0.29)
1^+	25.10(1, 0, 0)	1.21 (0.36, 0.49, 0.15)	0.53 (0.29, 0.46, 0.26)	0.39 (0.26, 0.44, 0.30)	0.33 (0.24, 0.43, 0.33)
2^+	36.10(1, 0, 0)	1.20 (0.23, 0.31, 0.46)	0.65 (0.21, 0.33, 0.46)	0.52 (0.20, 0.34, 0.46)	0.46 (0.19, 0.34, 0.47)
3^+	10.98(1, 0, 0)	0.43 (0.23, 0.31, 0.46)	0.25 (0.24, 0.32, 0.44)	0.20 (0.25, 0.33, 0.42)	0.18 (0.25, 0.33, 0.42)
4^+	7922.09(1, 0, 0)	3.93 (0.06, 0.17, 0.77)	1.03 (0.13, 0.29, 0.59)	0.70 (0.17, 0.31, 0.52)	0.57 (0.18, 0.32, 0.49)
5^+	415.67(1, 0, 0)	0.42 (0.06, 0.17, 0.77)	0.21 (0.13, 0.29, 0.58)	0.19 (0.18, 0.31, 0.52)	0.18 (0.20, 0.32, 0.48)
6^+		66.55 (0.02, 0.07, 0.91)	2.89 (0.03, 0.13, 0.84)	1.22 (0.05, 0.21, 0.74)	0.82 (0.09, 0.26, 0.65)
7^+		0.82 (0.02, 0.07, 0.91)	0.09 (0.03, 0.13, 0.84)	0.08 (0.05, 0.21, 0.74)	0.09 (0.09, 0.26, 0.65)
8^+		1319.19 (0.02, 0.05, 0.93)	11.90 (0.01, 0.07, 0.92)	2.87 (0.01, 0.10, 0.89)	1.44 (0.02, 0.13, 0.84)
Expt.	2.57±0.39	0.57±0.13	0.37±0.09		<0.37

not observed due to the low statistics and the small detection efficiency. Thus, the multiplicity 1 and 2 data are found to be consistent.

F. Decay widths

The theoretical decay branches of the various decay channels were calculated using R-matrix penetrabilities [22]. For neutron decay from an initial ^{14}C state feeding a ^{13}C state, the decay width is given by

$$\Gamma_{^{13}C[J_f]} = \sum_{j_n \ell_n} \Gamma^{J_i}_{J_f j_n \ell_n}. \tag{6}$$

Here $\Gamma^{J_i}_{J_f j_n \ell_n} = 2\gamma^2 P_\ell$, where P_ℓ is the JWKB penetration factor of Ref. [22] and γ^2 is the reduced width. For the purpose of comparison γ^2 has been assumed to be 1. J_i is the total angular momentum of the parent nucleus and J_f is the angular momentum of the daughter nucleus. The permissible angular momentum combinations $(j_n \ell_n)$ for the outgoing neutron are subject to the condition $\vec{J}_i = \vec{J}_f + \vec{j}_n$ and ℓ_n is either even or odd depending on the transition. The decay branches were calculated for each allowed neutron decay channel of the excited ^{14}C states of interest. The ratios of the decay branches associated with two different decay channels were then calculated over a range of J_i^π values.

The decay branch ratio for the neutron decay of the $^{14}C^*$ to the ^{13}C ground state ($1/2^-$) as a fraction of the neutron decay to any of the first three excited states ($1/2^+$, $3/2^-$, $5/2^+$), is given by

$$R = \frac{\Gamma_{^{13}C[\frac{1}{2}^-]}}{\Gamma_{^{13}C[\frac{1}{2}^+]} + \Gamma_{^{13}C[\frac{3}{2}^-]} + \Gamma_{^{13}C[\frac{5}{2}^+]}}. \tag{7}$$

Here the decay branches of the first three excited states are summed together as they were experimentally unresolved. The ratios were calculated for $J_i = 0$ to 8 for both the even and odd parity states and are shown in Table IV. Also shown are the associated experimental relative branching ratios calculated from the absolute branching ratios of Table II.

The theoretical and the experimentally determined ratios were then compared to provide information on the spin, parity and possible single particle structure of the decaying ^{14}C state. Differences between the ratios also provides information on the relative reduced widths as γ^2 has been assumed to be 1.

For the α-decay from an initial $^{14}C^*$ state feeding a ^{10}Be final state, the decay branches were calculated for each allowed α-decay channel and various ratios of the decay branches were calculated. The ratio of the α-decay branch to the ^{10}Be ground state (0^+) as a fraction of the α-decay branch to the first excited state (2^+), is given by

$$R = \frac{\Gamma_{^{10}Be[0^+]}}{\Gamma_{^{10}Be[2^+]}}. \tag{8}$$

Table V shows these ratios for $J^\pi = 0$ to 8 for natural parity states. Note that the α-decay of an unnatural parity state to the ^{10}Be ground state is forbidden.

Table VI shows the ratios of the neutron decay branch to the ^{13}C ground state as a fraction of the α-decay branch to the

TABLE V. Theoretical ratios of the α-decay branch to the ^{10}Be[0^+] ground state as a fraction of the α-decay branch to the first excited state (2^+). Also shown are the associated experimental relative branching ratios.

J_i^π	E_x (MeV)	
	18.6	21.4
0^+	3.56	1.74
1^-	1.68	0.88
2^+	0.96	0.57
3^-	1.07	0.63
4^+	1.14	0.68
5^-	1.15	0.68
6^+	1.21	0.58
7^-	1.39	0.47
8^+	1.71	0.41
Expt.	<0.33	<0.15

^{10}Be ground state ($\Gamma_{^{13}\mathrm{C}[1/2^-]}/\Gamma_{^{10}\mathrm{Be}[0^+]}$) and the ratios of the decay branch to the ^{13}C ground state compared to the decay branch to the first excited state in ^{10}Be ($\Gamma_{^{13}\mathrm{C}[1/2^-]}/\Gamma_{^{10}\mathrm{Be}[2^+]}$). These ratios provide information on the α-cluster content of a state.

IV. DISCUSSION OF THE EXCITED ^{14}C STATES

The present spectrum of the excited states of ^{14}C with $E_x > 11.66$ MeV is summarized in Table VII. The fifth panel shows the ^{14}C states which have been observed to decay via α-emission.

The ^{14}C states which are strongly populated in the two-neutron stripping reaction depend sensitively on dynamical matching conditions [29] and have been dominantly connected to stretched two-neutron configurations [30]. Such configurations are built by coupling the ^{12}C ground state with the two stripped neutrons which can occupy a combination of various orbits. The population strength of these orbits have been examined by Bohlen *et al.* [30]. The population of the $s_{1/2}$ orbital is very weak, the population of states containing $p_{1/2}$ and $d_{3/2}$ components are expected to be medium and the $d_{5/2}$ is expected to be strong. At higher ^{14}C excitation energies there will also be combinations with the $f_{7/2}$ which is also expected to be strongly populated. As an example, the 6.73 and 10.74 MeV states have ($^{12}\mathrm{C}_{\mathrm{g.s.}} \otimes p_{1/2} \otimes d_{5/2}$) and ($^{12}\mathrm{C}_{\mathrm{g.s.}} \otimes d_{5/2} \otimes d_{5/2}$) configurations, respectively. Thus, one would expect these two states to be strongly populated in the two-neutron stripping reaction, as confirmed by an examination of Fig. 1.

Some of the ^{14}C* states at higher excitation energies which are less strongly populated can be related to core excitations ($^{12}\mathrm{C}^*_{2^+}$ and $^{12}\mathrm{C}^*_{3^-}$). For a 2^+ core excitation, the states would be populated in a multistep process, the first step being the collective excitation of the system followed by the transfer of the two neutrons into the final orbits [31]. Again the matching conditions favor the population of stretched configurations of the two neutrons in the final state and high-spin states.

Below, is a list of some of the individual ^{14}C* states populated in the two-neutron transfer reaction. The population and decay characteristics of the states, along with the penetrability ratio calculations, are used to extract information on their spins, parities and configurations. A summary of the results can be found in Table VIII. The third column shows the predicted excitation energies of the ^{12}C core plus two-neutron configurations which have been calculated by von Oertzen *et al.* [18] using the simple shell-model approach of Chan [32,33].

A. 11.73 MeV

The 11.73 MeV state is observed to neutron decay to both the ^{13}C $1/2^-$ ground state and the $1/2^+$ first excited state with a ratio of 2.57 ± 0.39. From Fig. 6 it is evident that these are the only two decay channels available for this state. In Ref. [18]

TABLE VI. Theoretical ratios of the neutron decay branch to the ^{13}C ground state as a fraction of the α-decay branch to the ^{10}Be ground state ($\Gamma_{^{13}\mathrm{C}[1/2^-]}/\Gamma_{^{10}\mathrm{Be}[0^+]}$) and the ratio of the decay to the ^{13}C ground state compared to the decay to the first excited state in ^{10}Be ($\Gamma_{^{13}\mathrm{C}[1/2^-]}/\Gamma_{^{10}\mathrm{Be}[2^+]}$). Also shown are the associated experimental relative branching ratios.

E_x (MeV)	12.96	14.87	16.72	18.6	21.4	16.72	18.6	21.4
J_i^π			$\frac{\Gamma_{^{13}\mathrm{C}[\frac{1}{2}^-]}}{\Gamma_{^{10}\mathrm{Be}[0^+]}}$				$\frac{\Gamma_{^{13}\mathrm{C}[\frac{1}{2}^-]}}{\Gamma_{^{10}\mathrm{Be}[2^+]}}$	
0^+	35.79	2.25	1.54	1.32	1.18	89.57	4.69	2.05
1^-	162.35	5.43	3.33	2.76	2.41	43.81	4.64	2.12
2^+	716.31	8.10	3.84	2.94	2.48	18.88	2.83	1.42
3^-		17.83	5.22	3.37	2.61	32.29	3.62	1.65
4^+		61.32	9.47	4.47	2.90	91.93	5.09	1.97
5^-		295.36	24.95	7.68	3.59	431.68	8.84	2.42
6^+			86.30	18.13	5.50		21.99	3.20
7^-			299.12	50.86	10.89		70.57	5.13
8^+			863.09	132.42	24.20		225.92	9.81
Expt.	<3.4	1.31±0.35					<0.64	<0.08

TABLE VII. Proposed energy levels of ^{14}C for $E_x > 11.66$ MeV. The second panel shows the indicated levels taken from the ^{13}C(n, n) measurement of Ref. [23] and the latest compilation [24]. The fifth panel shows a compilation of the ^{14}C states which are observed to decay via α-emission. Evidence for the α-decay of these states is from ^{7}Li(^{9}Be, ^{10} Be $+ \alpha$) [25], ^{14}C(^{13}C, ^{10} Be $+ \alpha$) [26] and ^{14}C(^{14}C, ^{10} Be $+ \alpha$) [27] measurements.

This work		[23,24]			$2n$ transfer [18]		^{13}C$(\vec{p}, \pi^+)$ [28]		^{9}Be(^{7}Li,d) [18]		States which α-decay [25–27]	
E_x (MeV)	J^π	E_x (MeV)	J^π	Ref.	E_x (MeV)	J^π	E_x (MeV)	J^π	E_x (MeV)	J^π	E_x (MeV)	Ref.
		11.666	4^-	[24]	11.66	4^-	11.7	4^-	11.66	4^-		
11.73	$0^-, 1^-, 2^-$	11.73	5^-	[24]	11.73(3)	4^+			11.73	4^+		
		11.9(3)	(1^-)	[23]								
		12.20	1^-	[23]								
		12.61	2^-	[23]					12.58	(3^-)		
		12.863		[24]					12.86			
12.96	$0^-, 2^-, 3^-$	12.963	(3^-)	[24]	12.96(4)	3^-	12.96		12.96			
		(13.50)		[24]								
		13.7	2^-	[23]	13.7(1)		13.56					
14.1					14.0(1)				14.03		14.3(1)	[27]
		14.63	(1^-)	[23]	14.67(5)	6^+			14.67	6^+		
		14.717	4^+	[23]								
14.87	5^-	14.91	(1^+)	[23]	14.87(4)	5^-	14.87	5^-	14.87	5^-	14.8(1)	[25–27]
		15.20	4^-	[24]					15.18	(5^-)		
		(15.37)		[24]								
		15.44		[24]					15.40	(2^+)		
		15.56	3^-	[23]							15.55(10)[a]	[25,27]
15.75		15.8	(1^-)	[23]	15.75(8)							
		15.91	4^+	[23]							15.9	[26]
		(16.02)		[24]								
		16.43		[24]	16.4(1)	(6^+)			16.43	6^+	16.43(10)	[25–27]
		(16.57)		[24]					16.53	(2^+)		
16.72		16.715	(1^+)	[24]	16.72(5)	(6^+)			16.72	(1^+)		
		17.30	4^-	[24]			17.3	4^-	17.30	4^-	17.3(1)	[27]
17.5		(17.5)	(1^+)	[24]	17.5(1)				17.52	(2^+)		
		17.95		[24]					17.91	(2^+)		
		18.10		[24]					18.03	(7^-)	(18.1)	[27]
							18.53	(4^-)	18.39		18.5(1)	[25,26]
18.6	$2^-, 4^-, 6^-$				18.6(1)				18.60		18.6(1)	[27]
									19.14		(19.07(1))	[25–27]
											(19.3(1))	[27]
					19.8(1)	(2^+)			19.73	(2^+)	19.83(1)	[25–27]
		20.4		[24]					20.02		(20.3(1))	[27]
									20.75		20.6(1)	[25,27]
									21.00			
21.4					21.4(2)				21.41		21.43(1)	[25–27]
		22.1		[24]	22.5(3)						22.45(3)	[25,27]
					23.5		23.2				(23.15(1))	[25,27]
		24.3		[24]							24.0(3)	[25]
		24.5		[24]								

[a]Assigned a spin-parity of 3^- [27].

the state is given a possible (^{12}C$_{\text{g.s.}} \otimes p_{1/2} \otimes f_{7/2}$) or (^{12}C$_{\text{g.s.}} \otimes d_{5/2} \otimes d_{3/2}$) configuration. For the ($p_{1/2} \otimes f_{7/2}$) configuration the neutron decay to the $1/2^+$ ^{13}C state is suppressed and in the ($d_{5/2} \otimes d_{3/2}$) configuration the decay to the $1/2^-$ is similarly less probable. For both decays to occur strongly one of the transferred neutrons must be in an even parity orbit and the other neutron in an odd parity orbit. This indicates that it is a negative parity state. The experimental width of the state is 30 keV.

An examination of the penetrability calculations of Table IV suggests that the state is associated with a spin 0^-, 1^- or 2^-. From the arguments given above, the original spin-parity

TABLE VIII. A summary of the properties of various excited ^{14}C states populated in the two-neutron transfer reaction. The configurations are based on a ^{12}C core, in either the ground state or first excited state (2^+), coupled to the two stripped valence neutrons which occupy various orbits. The theoretically calculated excitation energies associated with the configurations and the experimental total decay widths are taken from Ref. [18]. The spins and parities show the allowed values determined from this work. The 11.73 MeV state has two possible configuration entries which are consistent with the ^{14}C excitation energy.

E_x (MeV)	J^π	Neutron conf. $^{12}\mathrm{C} \otimes (nlj) \otimes (nlj)$	E_x (MeV) Ref. [18]	Width (keV) Ref. [18]
11.73	$1^-, 2^-$	(g.s.)$\otimes p_{1/2} \otimes d_{3/2}$	11.43	30
11.73	$0^-, 1^-, 2^-$	$(2^+) \otimes p_{1/2} \otimes d_{5/2}$	11.52	30
12.96	$0^-, 2^-, 3^-$	$(2^+) \otimes p_{1/2} \otimes d_{5/2}$	11.52	25
14.87	5^-	$(2^+) \otimes p_{1/2} \otimes d_{5/2}$	11.52	35
16.72		(g.s.)$\otimes d_{5/2} \otimes f_{7/2}$	17.83	60
18.6	$2^-, 4^-, 6^-$			100
21.4				550

assignments of 4^+ [18] and 5^- [23] have to be considered to be wrong. The narrow width of the state and the spin and parity assignments coupled with the energy calculations of the ^{12}C core plus two-nucleon model of [18] show that the properties of the state are consistent with the ($^{12}\mathrm{C}_{2^+} \otimes p_{1/2} \otimes d_{5/2}$) or ($^{12}\mathrm{C}_{\mathrm{g.s.}} \otimes p_{1/2} \otimes d_{3/2}$) configurations. For the ($^{12}\mathrm{C}_{\mathrm{g.s.}} \otimes p_{1/2} \otimes d_{3/2}$) configuration the allowed spins are 1^- or 2^- and for the ($^{12}\mathrm{C}_{2^+} \otimes p_{1/2} \otimes d_{5/2}$) configuration all three spin values are allowed.

The weaker population of the state, in regards to its neighbours with $d_{5/2}$ components, suggests it has a ($^{12}\mathrm{C}_{\mathrm{g.s.}} \otimes p_{1/2} \otimes d_{3/2}$) configuration, as these two orbitals are only populated with a medium strength in the two-neutron transfer reaction. The narrow width of the state suggests a tentative spin-parity assignment of 2^-.

B. 12.96 MeV

This state is observed to neutron decay to the ^{13}C ground state and the first three excited states with a ratio of 0.57 ± 0.13. The relatively narrow width (25 keV) and strong population of the state suggests that it has a ($^{12}\mathrm{C}_{2^+} \otimes p_{1/2} \otimes d_{5/2}$) configuration and a negative parity. From Table IV the state would be associated with spins of 0^- to 4^-. The cross section and analyzing power angular distributions of Ref. [28] exclude the 1^- and the 4^-. This state has previously been observed in a number of reactions [18,23,28,34–36] and has been given a tentative spin-parity assignment of 3^- from the results of a $^{14}\mathrm{C}(\alpha, \alpha')$ study [37].

C. 14.87 MeV

This state has been observed in the $^{13}\mathrm{C}(p, \pi)$ reaction [28,38] where it was assigned a spin-parity of 5^-. It is not observed in the $^{14}\mathrm{C}(e, e')$ [39] and $^{14}\mathrm{C}(\pi, \pi')$ [40,41] measurements; supporting the assignment of a 5^- configuration which cannot be reached by $1p1h$ excitations from the ground state of ^{14}C. It can thus be clearly described as a core excitation and it is demonstrated to be the analog of a 5^- state in ^{14}N. Thus it is proposed to have a ($^{12}\mathrm{C}_{2^+} \otimes p_{1/2} \otimes d_{5/2}$) configuration [28,38] and consequently a negative parity. The state has a considerable width for α-decay to the ground state of ^{10}Be. Such a decay is only allowed for natural parity states. The ratio for the neutron decay to the ground state to the decay to the first three excited states is 0.37 ± 0.09. A comparison with Table IV suggests that the state can be assigned a spin 1^-, 3^-, or 5^-. The cross section and analyzing power angular distributions of Ref. [28] exclude the possibility of the 1^- and 3^- spins. Thus, a spin of 5^- would be indicated for this state in agreement with the previous measurements [18,28].

Another possible configuration would be ($^{12}\mathrm{C}_{gs} \otimes p_{1/2} \otimes f_{3/2}$). Such a configuration would have positive parity and would only strongly decay to negative parity states ($1/2^-$ and $3/2^-$) in ^{13}C. However, this configuration would favor decay to the ground state for positive, natural, parity states and can thus be excluded.

From the penetrability calculations of Table VI, it is evident that neutron decay is favored over α-decay. For a spin of 5^- the simple barrier penetrability argument indicates that it is 215 times more favorable for the 14.87 MeV state to neutron decay to the ^{13}C ground state than α-decay to the ^{10}Be ground state. Thus, the experimental ratio of 1.31 ± 0.35 demonstrates that this state has a very large α-decay width indicating a cluster structure. This state has previously been linked to an oblate rotational cluster-band [18].

D. 16.72 MeV

This state is not observed to neutron decay to the ground state of ^{13}C. This suggests that it does not contain a strong $p_{1/2}$ component. This is consistent with the previously assigned $[^{12}\mathrm{C}_{\mathrm{g.s.}} \otimes d_{5/2} \otimes f_{7/2}]_{6^-}$ configuration of Ref. [18]. The state is not observed to α-decay to the ground state of ^{10}Be, suggesting that it has unnatural parity; this is also consistent with the previously assigned spin-parity of 6^-. An examination of Table IV shows that unnatural parity states favor neutron decay to excited states. Again this is consistent with the decay characteristics of the state.

E. 18.6 MeV

The neutron decay of this state proceeds mostly to the first three excited states in ^{13}C. The state has a substantial width for α-decay to the first excited state in ^{10}Be[2^+]. The decay to the ^{10}Be[0^+] ground state is very weak if present at all. This is in contrast with Soić *et al*. [25] in which a broad state at 18.5 MeV was observed to have a substantial width for α-decay to both the ^{10}Be[2^+] and ^{10}Be[0^+]. This broad structure has previously been associated with both the 18.39 and 18.6 MeV states in two-neutron transfer reactions [18]. It must now be assumed that the state in Ref. [25] is the 18.39 MeV state which has been observed in various other measurements [18,26,28,41] and the present structure is the 18.6 MeV state. This structure may still involve several states, however, if it is a single state its broad width suggests that it has a low spin. The fact that it does not decay to the ^{10}Be[0^+] indicates that it has unnatural parity.

An examination of Table IV suggests that the state is associated with spins 2^-, 4^-, or 6^-. It is also evident that an unnatural parity state strongly favors neutron decay to excited states, as was experimentally observed. This state is populated in the ^{13}C(p,π^+) [28,38] and ^{14}C(π,π') [40,41] reactions, indicating a core excitation. It has previously been given a tentative spin-parity assignment of 6^- [18].

From Table VI it is evident that neutron decay to the ground state is favored over α-decay to the 2^+ in terms of the penetrability factors. Thus, the fact that α-decay is favored indicates that this state has a large α-decay width and is a possible cluster-structure candidate.

F. 21.4 MeV

This state has previously been observed as a broad structure in a number of reactions [18,25,26,28,41,42]. The large width (550 keV) suggests that it has a component with low spin. However, it may involve several states. It is seen to α-decay to both the 2^+ and the group of states at $\sim$6 MeV but the decay to the 0^+ ground state is not observed. This is consistent with a previous decay study using the ^{7}Li(^{9}Be,^{14}C $\rightarrow$ ^{10}Be+α) reaction [25]. The state is not observed to neutron decay. The large α-decay width suggests that it is a possible cluster state.

V. CONCLUSIONS

The decay modes and associated branching ratios of various excited ^{14}C states populated in the ^{12}C(^{16}O,^{14}O)^{14}C reaction have been studied. The strong dependence of the transfer cross section on dynamical matching conditions for different final configurations has been used to make tentative configuration assignments for many of the observed states. Theoretical decay branch ratios have been calculated from barrier penetration factors and have been used to provide information on the spins, parities, and single-particle configurations of the states.

The 14.87, 18.6, and 21.4 MeV states have been shown to possess large α-decay widths and are possible cluster structure candidates. The 16.72 MeV state has no α-decay width and appears to have a single-particle structure. The 11.73 and 12.96 MeV states lie close to the ^{10}Be+α decay threshold and are thus not seen to α-decay. Thus, it is hard to determine the nature of their structure.

The present measurements of the partial widths may be combined with subsequent measurements of spins to provide definitive evidence for the cluster nature of the states. Such measurements are planned for the near future.

ACKNOWLEDGMENTS

The authors would like to thank the staff members of the Hahn-Meitner-Institut for their assistance in running the experiments. We acknowledge the financial support of the U.K. Engineering and Physical Sciences Research Council (EPSRC).

[1] B. Buck, H. Friedrich, and C. Wheatley, Nucl. Phys. **A275**, 246 (1977).
[2] J. Hiura and R. Tamagaki, Suppl. Prog. Theor. Phys. **52**, 25 (1972).
[3] Y. Kanada-En'yo, H. Horiuchi, and A. Doté, Phys. Rev. C **60**, 064304 (1999).
[4] W. von Oertzen, Z. Phys. A **354**, 37 (1996).
[5] W. von Oertzen, Z. Phys. A **357**, 355 (1997).
[6] W. von Oertzen, Nuovo Cimento **110A**, 895 (1997).
[7] M. Freer, J. C. Angélique, L. Axelsson, B. Benoit, U. Bergmann, W. N. Catford, S. P. G. Chappell, N. M. Clarke, N. Curtis, A. D'Arrigo *et al*., Phys. Rev. Lett. **82**, 1383 (1999).
[8] M. Freer, J. C. Angélique, L. Axelsson, B. Benoit, U. Bergmann, W. N. Catford, S. P. G. Chappell, N. M. Clarke, N. Curtis, A. D'Arrigo *et al*., Phys. Rev. C **63**, 034301 (2001).
[9] M. Freer, J. C. Angélique, L. Axelsson, B. Benoit, U. Bergmann, W. N. Catford, S. P. G. Chappell, N. M. Clarke, N. Curtis, A. D'Arrigo *et al*., Phys. Rev. C **64**, 019904(E) (2001).
[10] M. Freer, E. Casarejos, L. Achouri, C. Angulo, N. I. Ashwood, N. Curtis, P. Demaret, C. Harlin, B. Laurent, M. Milin, *et al*., Phys. Rev. Lett. **96**, 042501 (2006).
[11] Y. Kanada-En'yo, H. Horiuchi, and A. Ono, Phys. Rev. C **52**, 628 (1995).
[12] Y. Kanada-En'yo and H. Horiuchi, Phys. Rev. C **52**, 647 (1995).
[13] A. Doté, H. Horiuchi, and Y. Kanada-En'yo, Phys. Rev. C **56**, 1844 (1997).
[14] Y. Kanada-En'yo and H. Horiuchi, Phys. Rev. C **66**, 024305 (2002).
[15] Y. Kanada-En'yo, Phys. Rev. C **66**, 011303(R) (2002).
[16] Y. Kanada-En'yo and H. Horiuchi, Phys. Rev. C **68**, 014319 (2003).
[17] M. Milin and W. von Oertzen, Eur. Phys. J. A **14**, 295 (2002).
[18] W. von Oertzen, H. G. Bohlen, M. Milin, T. Kokalova, S. Thummerer, A. Tumino, R. Kalpakchieva, T. N. Massey, Y. Eisermann, G. Graw *et al*., Eur. Phys. J. A **21**, 193 (2004).
[19] A. G. Drentje, H. A. Enge, and S. B. Kowalski, Nucl. Instrum. Methods **122**, 485 (1974).

[20] C. A. Wiedner, M. Goldschmidt, and D. Rieck, Nucl. Instrum. Methods **105**, 205 (1972).
[21] M. Löffler, H. J. Scheerer, and H. Vonach, Nucl. Instrum. Methods **111**, 1 (1973).
[22] A. M. Lane and R. G. Thomas, Rev. Mod. Phys. **30**, 257 (1958).
[23] D. A. Resler, H. D. Knox, P. E. Koehler, R. O. Lane, and G. F. Auchampaugh, Phys. Rev. C **39**, 766 (1989).
[24] F. Ajzenberg-Selove, Nucl. Phys. **A523**, 1 (1991).
[25] N. Soić, M. Freer, L. Donadille, N. M. Clarke, P. J. Leask, W. N. Catford, K. L. Jones, D. Mahboub, B. R. Fulton, B. J. Greenhalgh *et al*., Phys. Rev. C **68**, 014321 (2003).
[26] D. Price, M. Freer, S. Ahmed, N. I. Ashwood, N. M. Clarke, N. Curtis, P. McEwan, C. J. Metelko, B. Novatski, S. Sakuta *et al*., Nucl. Phys. **A765**, 263 (2006).
[27] D. Price, M. Freer, N. I. Ashwood, N. M. Clarke, N. Curtis, L. Giot, V. Lima, P. McEwan, B. Novatski, N. A. Orr *et al*., Phys. Rev. C **75**, 014305 (2007).
[28] E. Korkmaz, S. E. Vigdor, W. W. Jacobs, T. G. Throwe, L. C. Bland, M. C. Green, P. L. Jolivette, and J. D. Brown, Phys. Rev. C **40**, 813 (1989).
[29] D. M. Brink, Phys. Lett. **B40**, 37 (1972).
[30] H. G. Bohlen, R. Kalpakchieva, B. Gebauer, S. M. Grimes, H. Lenske, K. P. Lieb, T. N. Massey, M. Milin, W. von Oertzen, C. Schulz *et al*., Phys. Rev. C **68**, 054606 (2003).
[31] W. von Oertzen and A. Vitturi, Rep. Prog. Phys. **64**, 1247 (2001).
[32] T. U. Chan, M. Agard, J. F. Bruandet, and C. Morand, Phys. Rev. C **19**, 244 (1979).
[33] T. U. Chan, Phys. Rev. C **36**, 838 (1987).
[34] P. R. Andrews, B. M. Spicer, G. G. Shute, V. C. Officer, J. M. R. Wastell, H. Nann, Q. Li, A. D. Bacher, D. L. Friesel, and W. P. Jones, Nucl. Phys. **A468**, 43 (1987).
[35] M. E. Clark and K. W. Kemper, Nucl. Phys. **A425**, 185 (1984).
[36] R. O. Lane, H. D. Knox, P. Hoffmann-Pinther, R. M. White, and G. F. Auchampaugh, Phys. Rev. C **23**, 1883 (1981).
[37] R. J. Peterson, H. C. Bhang, J. J. Hamill, and T. G. Masterson, Nucl. Phys. **A425**, 469 (1984).
[38] E. Korkmaz, L. C. Bland, W. W. Jacobs, T. G. Throwe, S. E. Vigdor, M. C. Green, P. L. Jolivette, and J. D. Brown, Phys. Rev. Lett. **58**, 104 (1987).
[39] R. A. Lindgren, J. Phys. (Paris), Colloq. **C4**, 433 (1984).
[40] D. B. Holtkamp, S. J. Seestrom-Morris, S. Chakravarti, D. Dehnhard, H. W. Baer, C. L. Morris, S. J. Greene, and C. J. Harvey, Phys. Rev. Lett. **47**, 216 (1981).
[41] D. B. Holtkamp, S. J. Seestrom-Morris, D. Dehnhard, H. W. Baer, C. L. Morris, S. J. Greene, C. J. Harvey, D. Kurath, and J. A. Carr, Phys. Rev. C **31**, 957 (1985).
[42] J. D. Brown, L. K. Herold, K. E. Luther, A. A. Middleton, M. L. Pitt, D. Barker, and S. M. Aziz, Phys. Rev. C **38**, 1958 (1988).